Applied Catalysis B: Environmental 301 (2022) 120787

Contents lists available at ScienceDirect

Applied Catalysis B: Environmental

journal homepage: www.elsevier.com/locate/apcatb

Heterotopic reaction strategy for enhancing selective reduction and synergistic oxidation ability through trapping Cr (VI) into specific reaction site: A stable and self-cleaning ion imprinted CdS/HTNW photocatalytic membrane

Ziyang Lu [a,f,g,*], Guosheng Zhou [a], Bing Li [a], Yangrui Xu [a], Panpan Wang [a], Huan Yan [a], Minshan Song [b], Changchang Ma [c], Song Han [a], Xinlin Liu [d,e,**]

[a] Institute of Environmental Health and Ecological Security, School of the Environment and Safety Engineering, Jiangsu University, Zhenjiang 212013, Jiangsu, China
[b] School of Science, Jiangsu University of Science and Technology, Zhenjiang 212003, Jiangsu, China
[c] Department of Chemistry, Dongguk University, Seoul 04620, South Korea
[d] School of Energy and Power Engineering, Jiangsu University, Zhenjiang 212013, Jiangsu, China
[e] Department of Mechanical & Materials Engineering, Portland State University, Portland, OR, USA
[f] Jiangsu Collaborative Innovation Center of Technology and Material of Water Treatment, Suzhou University of Science and Technology, Suzhou 215009, Jiangsu, China
[g] Department of Chemistry, University of Tennessee, Knoxville 37996, TN, USA

ARTICLE INFO

Keywords:
Heterotopic reaction strategy
Enhanced synergistic photocatalytic ability
Selective reduction of trapped Cr (VI)
Ion imprinted CdS/HTNW
Stable and self-cleaning membrane

ABSTRACT

Ion imprinted CdS/HTNW photocatalytic membrane (IM-Cd/HT membrane) was prepared by assembling the oxidation type $H_2Ti_nO_{2n+1}{\cdot}xH_2O$ nanowires (HTNW) and the reduction type ion imprinted CdS (IM-CdS) for the removal of Cr^{6+} and tetracycline. Due to the imprinted cavities, Cr^{6+} was preferentially adsorbed and trapped at specific reaction sites for reduction reactions under the interference of other ions, and the selective reduction coefficients reached 80.01-fold and 91.92-fold. More intriguingly, Cr^{6+} and tetracycline reacted on the IM-Cd/HT membrane in a heterotopic manner, Cr^{6+} migrated to IM-CdS for selective reduction, while tetracycline migrated to HTNW for synergistic oxidation, and there was no interference between the two reactions, thereby IM-Cd/HT membrane exhibited a good synergistic balanced removal effect for Cr^{6+} and tetracycline. Besides, the Cr^{6+} flux of IM-Cd/HT membrane reached about 2952 L m^{-2} h^{-1} bar^{-1}, and the rejection rate of Cr^{6+} was 62.02%. This study provides a reference for the design of functional self-cleaning membrane with good synergistic photocatalytic ability.

1. Introduction

In the process of the development of industry and agriculture, water resource pollution has been paid more and more attention [1–6]. Heavy metal ions and antibiotic residues are two of the most serious pollution at present [7–9]. Among many heavy metal ions, Cr^{6+} with high toxicity is more easily absorbed by the human body, and will lead to cancer, gene defects and other serious diseases with the enrichment of the food chain [10–13], which should be removed first. Meanwhile, TC is widely used as a broad-spectrum antibiotic, and its residues are difficult to be completely removed in water [14,15]. And long-term existence of tetracycline can easily lead to the production of resistance genes [7,16]. Therefore, it is necessary to remove Cr^{6+} preferentially and tetracycline residues simultaneously.

At present, some researchers have found that the removal effect of organic pollutants and Cr^{6+} can be effectively improved by photocatalytic technology under the coexistence of these two pollutants [17–19]. To this end, Zhao et al. combined the results to prepare the powder material $AgI/BiVO_4$ photocatalyst, which can realize the full utilization of photogenerated carriers under the coexistence of Cr^{6+} and TC [20]. However, there are still some problems, such as the synergistic removal mechanism of Cr^{6+} and TC by photocatalyst is not fully

* Corresponding author at: Institute of Environmental Health and Ecological Security, School of the Environment and Safety Engineering, Jiangsu University, Zhenjiang 212013, Jiangsu, China.
** Corresponding author at: School of Energy and Power Engineering, Jiangsu University, Zhenjiang 212013, Jiangsu, China.
E-mail addresses: luziyang126@126.com (Z. Lu), liuxl@ujs.edu.cn (X. Liu).

https://doi.org/10.1016/j.apcatb.2021.120787
Received 11 August 2021; Received in revised form 23 September 2021; Accepted 3 October 2021
Available online 7 October 2021

explained, the photocatalytic mode of removing Cr^{6+} and TC by photocatalyst is not universal, and the interference of other metal ions may exist. In addition, from the perspective of economic benefits, environmental protection and convenience, the recycling of powder photocatalytic materials is also an urgent problem to be solved [21–25].

Photocatalytic membrane technology, as a combination of membrane separation and photocatalysis, is often used to remove Cr^{6+} and tetracycline residues in water [26–29]. Membrane materials can also solve the recycling of powder materials, practical use of difficult problems [30,31]. Besides, on the one hand, membrane separation technology can remove pollutants through interception, which has low energy consumption and high efficiency [32,33]. On the other hand, photocatalytic technology can not only realize the self-cleaning and reuse of membrane, but also can photocatalyze pollutants to remove, which has the advantages of green and stability [34–36]. Compared with organic polymer membrane, inorganic membrane has excellent rigidity, hydrophilicity, chemical stability and mechanical stability, and can be used under more severe conditions [37,38]. Zhang et al. reported that inorganic TiO_2 nanowire membrane had good stability, and could separate and photocatalytic oxidize pollutants at the same time [39,40]. The substrate material $H_2Ti_nO_{2n+1}{\cdot}xH_2O$ nanowires (HTNW) with a length of tens of microns and a large number of hydroxyl groups are easy to form a membrane after filtration, and has good hydrophilicity [41]. As a basic material for preparing membrane materials, PVA has the advantages of excellent hydrophilicity, good mechanical properties, good heat and chemical resistance, excellent membrane forming performance and so on, which can strengthen the physical and chemical stability of HTNW membrane [42–44]. More importantly, because of the wide band gap and low valence band, HTNW are a typical oxidation type photocatalyst with good oxidation ability, which can realize the efficient oxidative degradation of TC. Meanwhile, to reduce Cr^{6+} efficiently, reduction type photocatalysts (such as the commonly used visible light photocatalyst CdS) can be introduced into HTNW system.

The heterotopic reaction can simultaneously realize the reduction and removal of Cr^{6+} on reduction type photocatalysts and the oxidation and removal of TC on oxidation type photocatalysts, so as to achieve the best reduction and oxidation performance of the two types of photocatalysts respectively. Theoretically, in the process of simultaneous removal of Cr^{6+} and TC, the strong reducing electrons in the conduction band of photocatalyst can reduce the high valence heavy metal ions, and the strong oxidizing holes in the valence band can oxidize the organic pollutants [17,18,20,31,45,46]. But, in the actual process, it is difficult to efficiently achieve simultaneous action of heavy metal ions and organic pollutants due to the characteristics of non-selective attack of electrons and holes [47]. Meanwhile, Cr^{6+} and TC in the solution are evenly distributed. It is difficult for Cr^{6+} to exist only on the reduction type photocatalyst, and it is also difficult for TC to exist only on the oxidation type photocatalyst. Therefore, the reduction reaction of Cr^{6+} is trapped at the surface of the CdS, and the degradation reaction of TC is limited to HTNW, which can realize the heterotopic reaction of Cr^{6+} and TC and reduce the mutual interference between Cr^{6+} and TC.

Ion imprinting technology can realize the selective adsorption of Cr^{6+} and limit the subsequent reaction to the specific site of ion imprinted cavities [48,49]. At present, the ion-imprinted POPD-$CoFe_2O_4$ photocatalyst and ion-imprinted $ZnFe_2O_4$ photocatalyst successfully prepared by He et al. in combination with the imprinting technology can preferentially adsorb and reduce heavy metal ions in the ion-imprinted cavities [19,45]. However, the synergistic removal of these two types of pollutants in the true sense was not realized because it was only tested in single solution. In particular, the TC degradation of these systems system was carried out inside the ion imprinted catalyst, which increased the great transfer resistance, resulting in the insufficient utilization of the oxidative degradation performance. Hence, the combination of imprinting technology and reduction type photocatalyst can realize the reaction of Cr^{6+} trap at the specific site of imprinted cavities without interfering with the oxidative degradation of TC on oxidation type photocatalyst. The heterotopic reaction can maximize the preferential reduction ability and oxidative degradation ability of the two types of photocatalysts. As far as we know, the removal of heavy metals and antibiotic residues by heterotopic reaction has not been reported.

Therefore, we combined the base membrane material HTNW and IM-CdS particles by blending and suction filtration to quickly prepare Cr^{6+} ion imprinted CdS/HTNW membrane. The materials were characterized in detail by XRD, SEM, TEM, XPS, FT-IR, BET, etc. The photocatalytic activity, the selective removal of Cr^{6+} performance, the effect of synergistic removal of Cr^{6+} and TC, the water flux, rejection rate, self-cleaning performance and recyclability of the membrane were explored. Most importantly, the heterotopic reaction mechanism of selective photocatalysis for synergistic removal of Cr^{6+} and TC was explained in detail.

2. Materials and methods

2.1. Reagents

P25, 2,2′-azobis(2-methylpropionitrile) (AIBN), hydrochloric acid (HCl), citric acid monohydrate ($C_6H_8O_7{\cdot}H_2O$), cadmium sulfide (CdS), diphenylcarbazide, absolute ethanol, potassium dichromate ($K_2Cr_2O_7$), copper sulfate pentahydrate ($CuSO_4.5H_2O$), sulfuric acid (H_2SO_4), acetone, 4-vinyl pyridine (4-VP), ethyleneglycol dimethacrylate (EGDMA), polyvinyl alcohol (PVA), filter-membrane (0.45 μm pore size), phosphoric acid (H_3PO_4), tetracycline (TC) and methylene blue (MB), deionized water (DW). Unless stated otherwise, all chemicals were analytical grade.

2.2. Synthesis

2.2.1. Synthesis of HTNW

0.5000 g P25 and 60 mL NaOH solution (10 mol/L) with stirring and sonication at ambient temperature for the homogeneous dispersion. The obtained suspension was poured into a 100 mL autoclave and heated at 180 °C for 48 h. Whereafter, the mixture was washed with 0.1 mol/L HCl and DW by centrifugation until neutral to remove sodium ions. Thereafter, the white solids were dried at 60 °C under vacuum for 12 h and finally ground into powder by mortar and pestle. The white powders are designated as HTNW.

2.2.2. Synthesis of ion imprinted CdS (IM-CdS)

IM-CdS were synthesized through microwave polymerization. Initially, 0.4000 g CdS was introduced in 30 mL acetone solution with sonication for 30 min. Then, 0.1940 g $K_2Cr_2O_7$ (Cr^{6+} ion as template ions) was dissolved in 50 mL acetone-DW mixed solution (acetone: DW = 3:2). Next, 1.05 mL 4-VP (as functional monomers) was added to the above solution and stirred for 1 h for prepolymerization, and 1.9 mL EGDMA (as cross-linking agents) and 0.080 g AIBN (as initiators) were added. Subsequently, the two solutions were introduced together into a 250 mL three-neck flask, and polymerized at 800 W and 70 °C for 120 min. After that, as-synthesized compound precipitations were collected through centrifugation and washed with DW and absolute ethanol. The next stage was the elution of those compounds with 0.2 mol/L NaOH solution to remove Cr^{6+} ion until it couldn't be detected. Thereafter, the compounds were washed with DW by centrifugation until neutral and dried at 60 °C under vacuum for 12 h (labeled as IM-CdS).

2.2.3. Synthesis of Cr(Ⅵ) ion imprinted CdS/HTNW membrane (IM-Cd/HT membrane)

IM-Cd/HT membrane was synthesized through simple vacuum filtration. 0.3000 g HTNW and 0.1500 g IM-CdS were scattered to 20 mL DW with sonication for 10 min. The mixture was poured in vacuum filtration with filter-membrane (0.45 μm pore size) for 5 min, and 2 mL 0.5 wt% PVA solution was introduced for 5 min. Thereafter, the light-yellow membrane was peeled off from filter-membrane and heated at

60 ℃ for 3 h (labeled as IM-Cd/HT membrane) (Scheme 1).

2.2.4. Synthesis of other membrane materials

The synthesis of CdS/HTNW membrane (Cd/HT membrane) was to replace IM-CdS in Part 2.5 with CdS, and the rest of the process was the same as that of IM-Cd/HT membrane. Similarly, non-imprinted CdS/HTNW membrane (NM-Cd/HT membrane) was synthesized only without $K_2Cr_2O_7$ in the process of IM-Cd/HT membrane.

2.3. Experimental methods

2.3.1. Photocatalysis experiment

The whole experiment was carried out in a 100 mL quartz beaker under dark or xenon lamp (180 W) condition. In the dark condition, a piece of prepared imprinted photocatalytic membrane (effective area: 12.57 cm^2) was scattered into 50 mL 20 mg/L TC or 20 mg/L Cr^{6+} single solution with pH = 2, and air at the rate of 100 mL/min was continuously injected and stirred. After the adsorption was stable for 30 min, turn on the lamp for next process. Within the next 60 min, 4 mL of solution was taken twice for detection. The concentration of TC was detected by UV–visible spectrophotometer at 356 nm wavelength. In addition, the concentration of Cr^{6+} was measured by diphenylcarbazide method [10]. The photocatalytic reduction rate (PRR) and photocatalytic degradation rate (PDR) of pollutants can be expressed as follows:

$$PRR = \left(\frac{C_0 - C_t}{C_0}\right) \times 100\% \quad (1)$$

$$PDR = \left(\frac{C_0 - C_t}{C_0}\right) \times 100\% \quad (2)$$

C_0 and C_t represent the pollutant concentration (mg/L) when the adsorption equilibrium is reached and when the light duration is t, respectively.

2.3.2. Selectivity experiment

In order to show that the prepared materials can selectively remove Cr^{6+} in complex water environment, two binary mixed pollutant solutions containing Cr^{6+} were used instead of the single solution in photocatalytic experiment. The two binary mixed pollutant solutions: ① 20 mg/L TC and 20 mg/L Cr^{6+} binary mixed solution; ② 20 mg/L Cu^{2+} and 20 mg/L Cr^{6+} binary mixed solution. The process of selectivity experiment was the same as that of photocatalysis experiment. Simply, in the dark, a piece of prepared imprinted photocatalytic membrane was added to 50 mL of pH = 2 binary mixed solution, and air at the rate of 100 mL/min was continuously injected and stirred. After the adsorption was stable for 30 min, turn on the lamp for next process. Within the next 60 min, 4 mL of solution was taken twice for detection. The concentration of tetracycline was detected by High Performance Liquid Chromatography (Agilent 1260 Infinity LC) (methanol: 0.1 wt% acetic acid = 60:40, flow rate: 1 mL/min, detection wavelength: 276 nm, chromatographic column: C18, particle size: 5 μm, 4.6 mm*250 mm). The concentration of Cr^{6+} was measured by diphenylcarbazide method. The content of Cu^{2+} was detected by Inductively Coupled Plasma Optical Emission Spectrometer (Shimadzu ICPE-9820). The selective removal coefficient of heavy metal ions (K_{ion}) and the selective removal coefficient of materials ($K_{material}$) can be expressed as follows:

$$K_{ion} = \frac{PRR_{(Cr^{6+})}}{PRR_{(Cu^{2+})}} \quad (3)$$

$$K_{material} = \frac{K_{ion(IM-Cd/HT\quad membrane)}}{K_{ion(other\quad membrane)}} \quad (4)$$

2.3.3. Cycle experiment

IM-Cd/HT membrane was used for a photocatalytic experiment in 20 mg/L Cr^{6+} single solution, then washed two times with DW. After 200 days of storage in room temperature air environment, the membrane was used for 5 times of repeated photocatalytic experiments on 20 mg/L Cr^{6+} single solution.

2.3.4. Membrane flux and rejection experiment

The whole experiment process was carried out in a negative pressure vacuum filter with a pressure value of 0.1 bar. The formula of flux and rejection is as follows:

$$J_W = \frac{V_W}{A \cdot \Delta t} \quad (5)$$

$$J_{Cr} = \frac{V_{Cr}}{A \cdot \Delta t} \quad (6)$$

J_W and J_{Cr} are the flux (L m^{-2} h^{-1}) of DW and solution containing Cr^{6+}, respectively, V_W and V_{Cr} are the volume (L) of pure water and solution containing Cr^{6+} passing through the membrane, respectively, A is the effective area (1.257×10^{-3} m^2) of the membrane, Δt is the time (h) required for the solution to pass through the membrane.

$$\text{Rejection} \quad \text{Rate} = \left(\frac{C_0 - C}{C_0}\right) \times 100\% \quad (7)$$

C_0 and C represent the concentration (mg/L) of Cr^{6+} in the original solution and the filtrate, respectively.

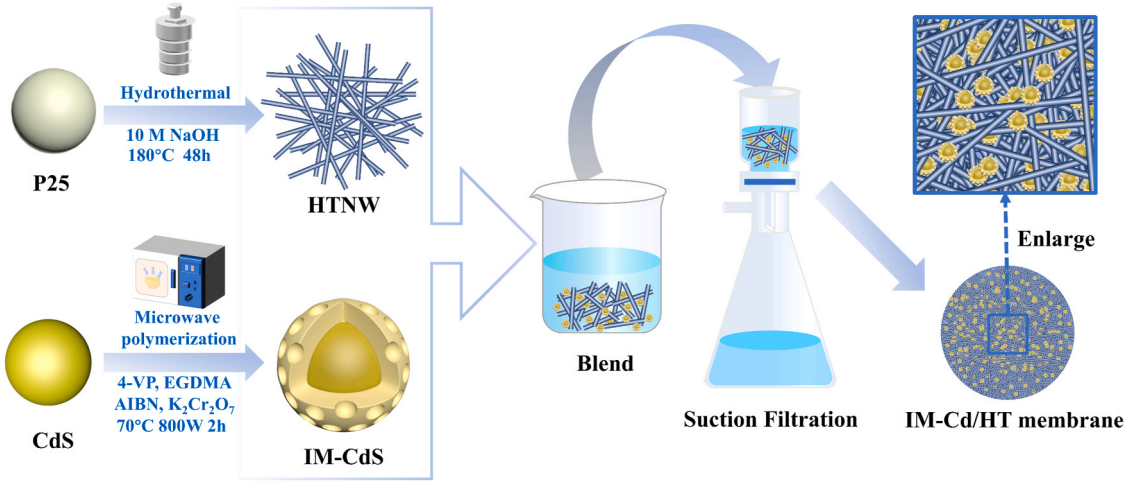

Scheme 1. Synthesis process of IM-Cd/HT membrane.

3. Results and discussion

3.1. Crystalline structure

The crystalline structures of several materials were shown in Fig. 1 through XRD characterization. The crystal structure of HTNW was not obvious, but the small peaks at 24.91° and 48.54° were consistent with previous studies [39]. Both CdS and IM-CdS materials had sharp diffraction peaks at the same position, which were consistent with the hexagonal CdS of the standard card PDF#77–2306 [50]. The various crystal planes corresponding to different diffraction peaks. This indicated that during the imprinting process of preparing IM-CdS with CdS, the crystal form of CdS did not change. The peak of Cd/HT membrane and IM-Cd/HT membrane were consistent with CdS, and the peak of HTNW could not be seen, because the peak of HTNW was relatively weak and it was more difficult to observe after recombination. In subsequent FT-IR, EDS and XPS experiments, the existence of HTNW was proved.

3.2. FT-IR

In Fig. 2, the absorption peak of the inorganic material HTNW at low frequencies of 1000 cm^{-1} - 500 cm^{-1} was ascribed to the Ti-O bond [51]. In addition, the peak at 3400 cm^{-1} was ascribed to the interaction of the hydroxyl groups of HTNW surface [52], and the strong and broad hydroxyl absorption band 3200 cm^{-1} was attributed to the interaction between Ti-OH [53]. After performing the imprinting process on CdS, IM-CdS added three new absorption peaks. The absorption band at 1616 cm^{-1} was considered to be the tensile vibration peak of the C═N bond in the pyridine group [54,55], and the absorption band at 1501 cm^{-1} and 1337 cm^{-1} were due to the 4-vinylpyridine ring [56]. This indicated that the surface of IM-CdS had 4-VP or its polymer, which was further proved by subsequent XPS, EDS and SEM characterization. It was observed that in the final material IM-Cd/HT membrane, the peak position remained unchanged but the peak intensity was reduced due to the addition of IM-CdS, while no polymer peak was found due to its low content.

3.3. Morphology

The morphology of the observed materials was shown in Fig. 3. In Fig. 3A and B, CdS and IM-CdS had the same morphology, and the morphology of CdS would not change during the imprinting process.

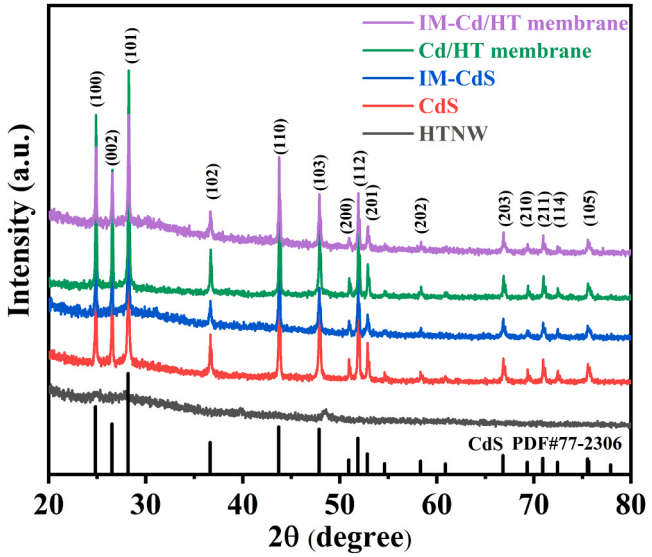

Fig. 1. The XRD pattern of different samples.

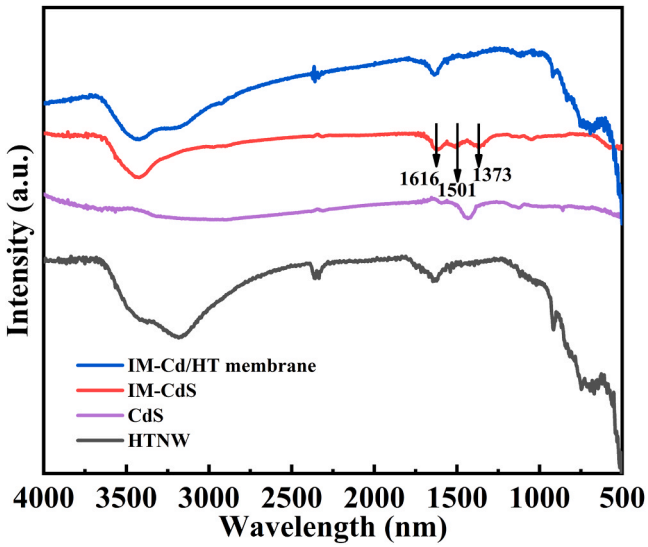

Fig. 2. The FT-IR pattern of different powder samples.

According to EDS element analysis in Table S1, the content of C, N and O in IM-CdS was increased relative to CdS, indicating the existence of imprinted polymer. This situation was further visualized in Fig. 3D, and it was obvious that there was a continuous uniform organic layer about 10 nm thick on the surface of IM-CdS to wrap CdS to form a core-shell structure. Combined with the results of FT-IR, it showed that 4-VP could be effectively polymerized to form a polymer after the microwave reaction and uniformly covered the surface of CdS. In addition, the morphology of the matrix material HTNW was shown in Fig. S1. HTNW was a 1D nanowire with a diameter of several hundred nanometers and a length of more than ten microns. This nanowire was beneficial to weaving into a stable inorganic photocatalytic membrane. After the mixed suction filtration of HTNW and IM-CdS, Fig. S2 showed that IM-CdS particles and HTNW coexist, and the non-detection of N element was caused by the low content. In Fig. 3E and F, a large number of IM-CdS particles uniformly existed in the cross network formed by HTNW, forming a stable IM-Cd/HT membrane structure, and a large number of contact surfaces were exposed, which was conducive to the subsequent stable photocatalytic process.

3.4. XPS

XPS was used to further confirm the surface structures of different materials (Fig. S3 and Fig. 4). As shown in Fig. 4A, the peaks of Ti $2p_{1/2}$ (463.04 eV) and Ti $2p_{3/2}$ (457.22 eV) in HTNW and IM-Cd/HT membrane split to 5.82 eV, indicating the positive tetravalent oxidation state of Ti element [57,58]. In addition, there was no structural change in HTNW during the whole synthesis process. The binding energy peaks of O element in HTNW at 530.78 eV and 528.69 eV were attributed to Ti—O bond and —OH bond on the sample surface, respectively [59,60]. The results showed that O element on IM-CdS surface mainly existed in EGDMA, and the peak of binding energy at 532.29 eV was ascribed to C═O bond and 530.66 eV was ascribed to C—O [59,61]. After the composite of the two materials, the O atom of IM-Cd/HT membrane contained the bond described above. Meanwhile, in the high-resolution spectrum of C 1s, the binding energy at 287.51 eV was attributed to C═N bond in pyridine group and C═O bond in EGDMA, the binding energy at 284.82 eV was attributed to C—N bond in 4-VP or EGDMA and C—O bond in EGDMA, and the peak at 283.60 eV corresponded to C—C bond, C—H bond and C═C bond in imprinted layer [59,61,62]. In addition, the N element in IM-CdS and IM-Cd/HT membrane did not shift. The above results showed that the imprinted polymer was successfully prepared, and the surface polymer did not change during the

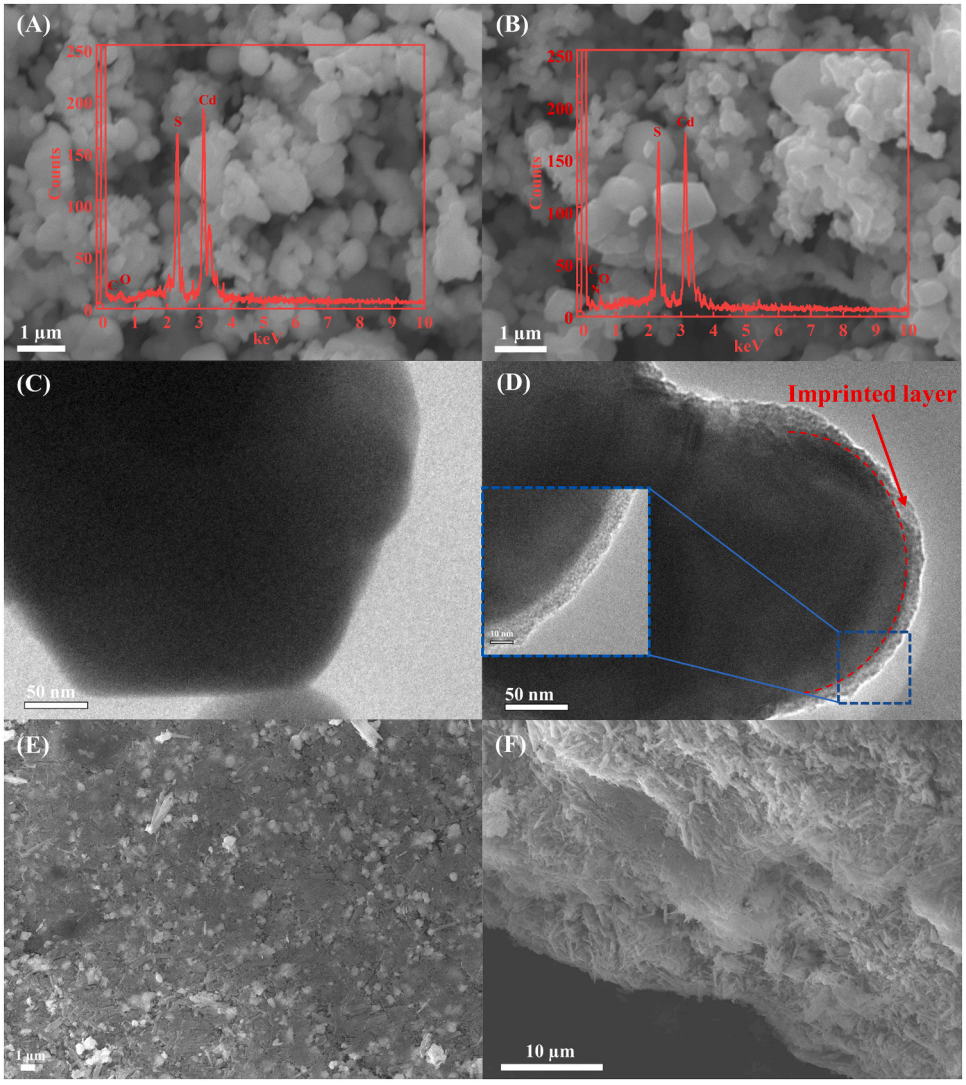

Fig. 3. The SEM pattern of CdS (A) and IM-CdS (B), the TEM pattern of CdS (C) and IM-CdS (D), and the top (E) and side (F) of IM-Cd/HT membrane. (The red chart inserted is EDS spectra and the blue dotted line box is enlarged).

synthesis process. For CdS, IM-CdS and IM-Cd/HT membrane, at 410.86 eV and 404.12 eV corresponding to $Cd3d_{3/2}$ and $Cd3d_{5/2}$, respectively, and at 161.51 eV and 160.39 eV corresponding to $S2p_{1/2}$ and $S2p_{3/2}$, respectively [23], their peak patterns did not change, but shifted to the position with small binding energy. This might be due to the imprinted polymer layer covering.

3.5. Nitrogen adsorption-desorption experiment

Nitrogen adsorption-desorption experiment can measure the BET specific surface area (S_{BET}) and pore size distribution of the material, which can effectively prove the possibility of the existence of imprinted cavities. At the same time, large S_{BET} was conducive to the contact and retention of contaminants [32]. As shown in Fig. 5, the S_{BET} of CdS, NM-CdS and IM-CdS were 2.66 m^2/g, 4.46 m^2/g and 10.06 m^2/g, respectively. The S_{BET} of NM-CdS relative to CdS has increased, which was caused by the coating of the organic polymer layer. In contrast, the S_{BET} of IM-CdS was further improved, and the average pore size (D_{APS}) was also reduced from 4.71 nm of NM-CdS and 5.42 nm of CdS to 3.94 nm. This was similar to the results in the previous literature [63]. The results show that during the imprinting process, the template ions were removed leaving a large number of imprinting cavities, which led to an increase in the S_{BET} and a decrease in the D_{APS}. In addition, the base membrane with HTNW had a larger S_{BET} of 33.00 m^2/g in Fig. S3. The preparation of IM-Cd/HT membrane helped to achieve the adsorption and retention of contaminants. The XRD, FT-IR, SEM, TEM, EDS, XPS and nitrogen adsorption-desorption experiment results indicated that the materials were successfully prepared.

3.6. UV-Vis DRS

The UV-Vis diffuse reflectance absorption spectra of different materials were obtained and demonstrated in Fig. 6A. The absorption edge of of HTNW is at 369 nm, and the light absorption range was in the ultraviolet region. The absorption edge of CdS was at 532 nm, which could effectively absorb visible light. After the imprinted polymer layer was coated with CdS, the edge of the absorption band of IM-CdS was red-shifted to 549 nm, which indicated that imprinted polymer could broaden the absorption capacity of visible light to a certain extent, which was beneficial to the photocatalytic reaction. After mixing HTNW and IM-CdS, the IM-Cd/HT membrane could make good use of visible light. The band gap was calculated according to the Tauc plot of $(\alpha h\nu)^2$ versus $h\nu$ [64–69]. The band gaps of HTNW and CdS were 3.64 eV and 2.38 eV, respectively, as demonstrated in Fig. 6B.

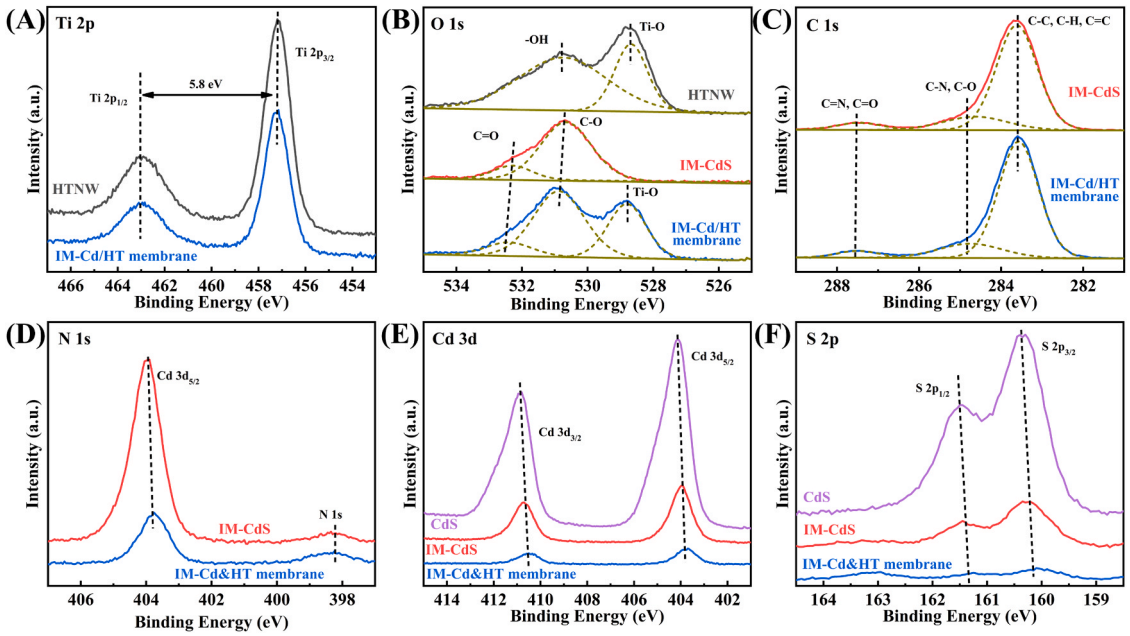

Fig. 4. XPS high-resolution spectra of different samples.

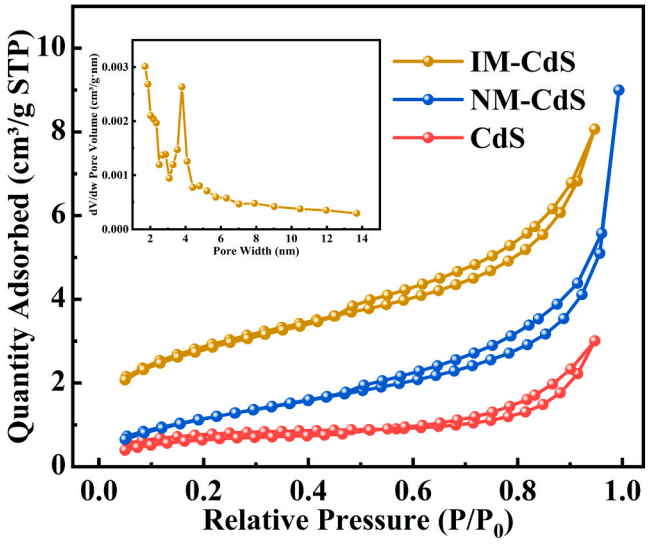

Fig. 5. The nitrogen adsorption-desorption experiment of different powder samples.

3.7. Photocatalytic performance and selectivity

To further approach the actual state of pollutant removal in water treatment, in addition to the removal of single pollutant solution, it is also used to remove binary mixed pollutant solution. Fig. 7A showed the removal of TC or Cr^{6+} from the single solution by HTNW membrane, Cd/HT membrane, NM-Cd/HT membrane and IM-Cd/HT membrane. The degradation rate of TC by the four membranes was about 20%, and TC was mainly degraded by HTNW. Meanwhile, the Cr^{6+} removal rate of HTNW membrane was 69.88%, and the reduction rate of membrane increased to 82% after mixing CdS materials, which reflected the effect of CdS on the reduction of Cr^{6+}.

Subsequently, the performance of synergistic removal of TC and Cr^{6+} was explored, and the results exhibited in Fig. 7B. Compared with the TC single solution, the degradation performance of TC in the solution of binary TC and Cr^{6+} was improved. This might be due to the consumption of photogenerated electrons by Cr^{6+}, which promoted the migration of photogenerated carriers and improved the oxidation performance [17,18,20]. However, in the binary solution, the reduction rate of HTNW was reduced by 16.41% compared with the single Cr^{6+} solution. This was because the adsorption of TC and Cr^{6+} was competitive with each other. The adsorption of TC on HTNW weakened the adsorption of Cr^{6+}, resulting in the reduction of Cr^{6+} removal efficiency. For Cd/HT

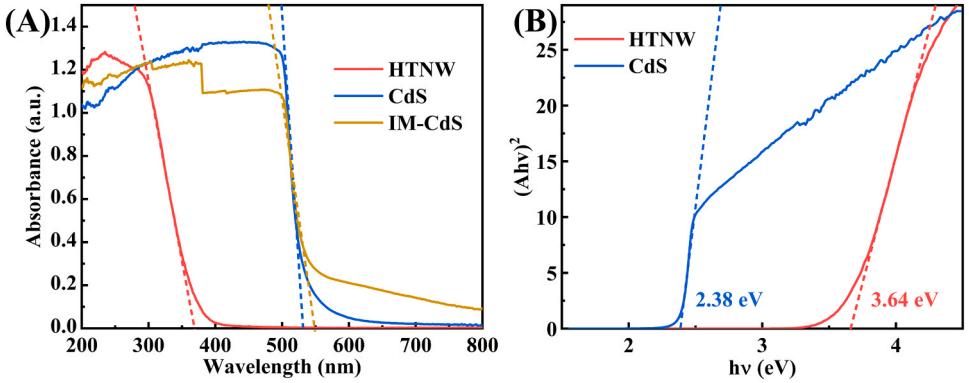

Fig. 6. The UV–vis DRS pattern (A) and Tauc curve (B) of different powder samples.

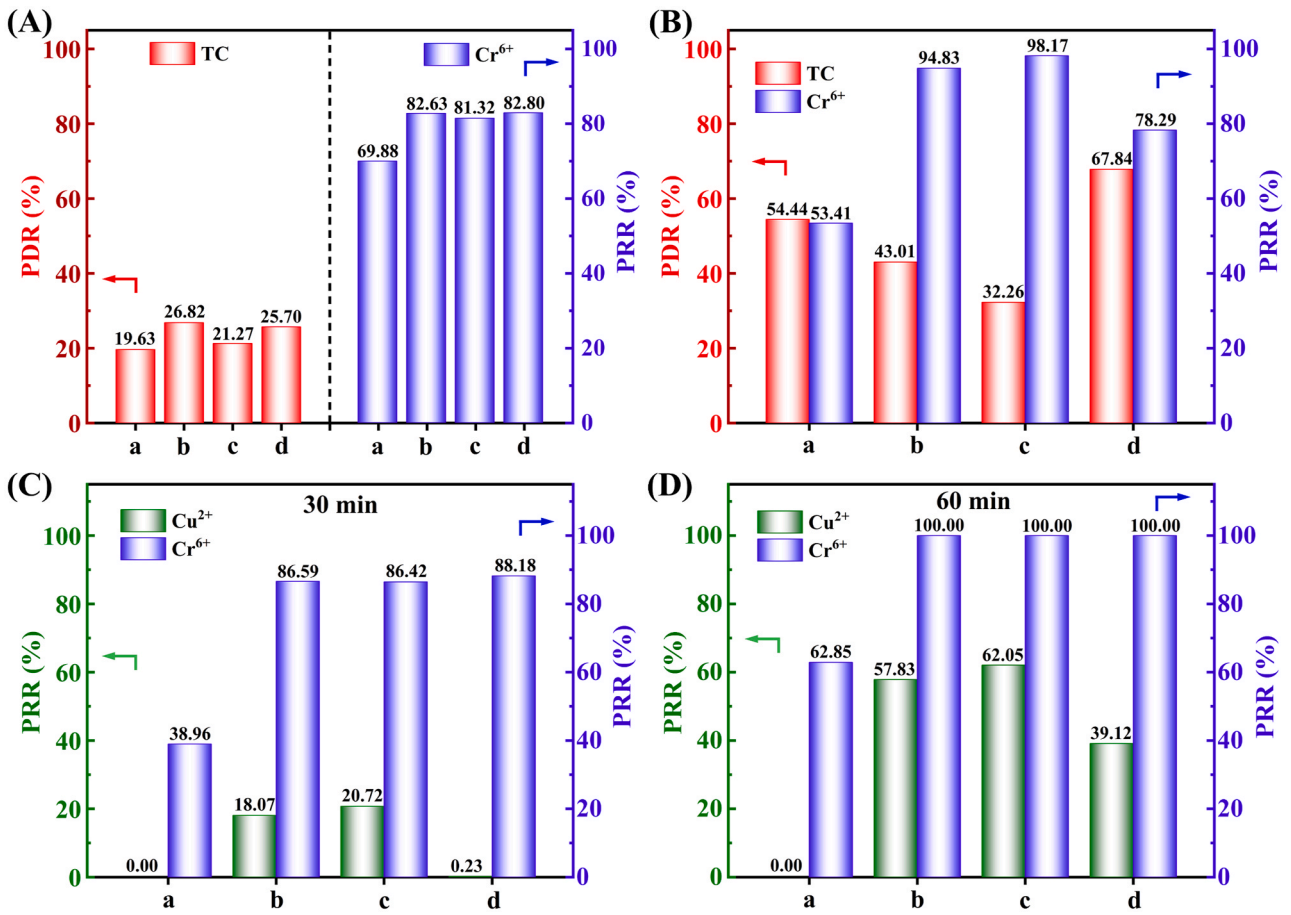

Fig. 7. Different membrane materials: Single solution for removing TC and Cr^{6+} (A), binary mixed solution for removing TC and Cr^{6+} (B), binary mixed solution for removing Cu^{2+} and Cr^{6+} at 30 min (C) and 60 min (D) (a. HTNW membrane, b. Cd/HT membrane, c. NM-Cd/HT membrane and d. IM-Cd/HT membrane).

membrane, a large number of CdS with good reducing property were loaded on the surface of the HTNW membrane. And the reduction of Cr^{6+} was increased to 94.83%. Meanwhile, the removal efficiency of TC reached 43.01%. Compared with the single TC or Cr^{6+} solution, the removal efficiency of TC and Cr^{6+} was improved, resulting in a certain degree of synergistic removal effect. However, compared with the HTNW membrane in binary TC and Cr^{6+} solution, the removal rate of TC decreased by 11.43%. This might be because the adsorption competition between Cr^{6+} and TC affected the adsorption effect of TC. The NM-Cd/HT membrane had the same photoactivity trend and mechanism with Cd/HT membrane for removing TC and Cr^{6+}. However, compared with Cd/HT membrane, the removal efficiency of TC with NM-Cd/HT membrane decreased and the reduction efficiency of Cr^{6+} increased. The cause of this phenomenon was demonstrated by photoelectrochemical experiment (Fig. S6). Due to the coating of organic polymer layer had good conductivity and the ability to promote electron transfer, which improved the reduction ability of the NM-Cd/HT membrane for Cr^{6+}. Finally, the IM-Cd/HT membrane could simultaneously maintain a good reduction rate of Cr^{6+} (78.29%) and a high removal rate of TC (67.84%). Compared with other membranes, IM-Cd/HT membrane had a good synergistic effect, which might be attributed to the occurrence of heterotopic reaction. Cr^{6+} was reduced in the imprinted cavities on the IM-CdS surface, while TC was oxidized on the HTNW surface. Meanwhile, due to the effect of imprinted layer, most of Cr^{6+} were enriched in a certain number of imprinted cavities and reduced, while the reduction of Cr^{6+} in the outer region was less, resulting in the reduction rate of Cr^{6+} in IM-Cd/HT membrane was slightly lower than that IM-Cd/HT membrane. Therefore, under the co-existence of TC and Cr^{6+}, especially due to the occurrence of heterotopic reaction, IM-Cd/HT membrane exhibited a good balanced removal effect for TC and Cr^{6+}, and the synergistic degradation of the two pollutants was realized.

The effect on selective preferential removal of Cr^{6+} was further discussed. The reduction rates of Cu^{2+} and Cr^{6+} at 30 min and 60 min were shown in Fig. 7C and D. HTNW membrane could not reduce Cu^{2+}, which might be because the reduction potential of HTNW was lower than that of Cu^{2+}/Cu [45]. In addition, Cu^{2+} occupied the active sites on HTNW surface, which reduced the reduction rate of Cr^{6+}. At 30 min, Cd/HT membrane and NM-Cd/HT membrane enhanced the reduction rate of Cu^{2+} and Cr^{6+} at the same time. However, because IM-Cd/HT membrane had an imprinted layer, it could achieve preferential reduction of Cr^{6+}, and basically no effect on Cu^{2+} reduction effect. The selective removal coefficients of IM-Cd/HT membrane relatived to Cd/HT membrane and NM-Cd/HT membrane were 80.01 and 91.92 respectively (Table 1), which were much higher than those reported in other literatures (Table S2). This further verified that IM-CdS could enrich and preferentially remove Cr^{6+}. The reduction performance of Cd/HT membrane, NM-Cd/HT membrane and IM-Cd/HT membrane in reducing Cr^{6+} in binary Cu^{2+} and Cr^{6+} solution was better than that in binary TC and Cr^{6+} solution and single Cr^{6+} solution, which might be

Table 1
Selective removal coefficients of different membranes at 30 min.

Sample	K_{ion}	$K_{material}$
Cd/HT membrane	4.79	80.01
NM-Cd/HT membrane	4.17	91.92
IM-Cd/HT membrane	383.39	–

due to the "benign competition" between Cu^{2+} and Cr^{6+} (Fig. S7). At 60 min, the reduction rate of Cr^{6+} by Cd/HT membrane, NM-Cd/HT membrane and IM-Cd/HT membrane reached 100%. The reduction rates of Cu^{2+} by Cd/HT membrane and NM-Cd/HT membrane was 57.83% and 62.05% respectively, while the reduction rate of Cu^{2+} by IM-Cd/HT membrane was only 39.12%. Above results further showed that the imprinted cavities could specifically adsorb Cr^{6+} and inhibit the reduction of Cu^{2+}. Therefore, Cr^{6+} was selectively and preferentially adsorbed and reduced by IM-Cd/HT membrane, which further confirmed the feasibility of heterotopic reaction.

In summary, the possible adsorption processes of TC and Cr^{6+} on different membrane surfaces in binary solution were shown in Fig. 8. The process of adsorption on HTNW membrane, Cd/HT membrane and NM-Cd/HT membrane was a disordered competitive reaction, while on IM-Cd/HT membrane was an ordered heterotopic reaction. In the presence of single photocatalyst HTNW (Fig. 8a), TC and Cr^{6+} would compete for the adsorption sites on HTNW surface simultaneously, and the removal of TC and Cr^{6+} would affect each other. Similarly, in the presence of double photocatalysts HTNW and CdS (Fig. 8b), the competition of adsorption sites occurred not only on the surface of HTNW, but also on the surface of CdS. The competitive adsorption process of NM-Cd/HT membrane was the same as that of Cd/HT membrane. In addition, to enhance contrast, a simple Ag/HTNW membrane was also explored, as presented in Fig. S8 and S9, the adsorption also belonged to disordered competitive reaction, and the reduction of Cr^{6+} would also be disturbed. Fig. 8C showed the possible reasons for the removal of Cr^{6+} and TC by IM-Cd/HT membrane in binary solution. Cr^{6+}could be selectively recognized by the imprinted cavities in the IM-CdS imprinted layer and preferentially adsorbed in the imprinted cavities, resulting in enhanced enrichment on IM-CdS, and reduced enrichment on HTNW. The decrease of Cr^{6+} enrichment on HTNW led to the decrease of the adsorption repulsion of HTNW to TC, more TC were adsorbed on the surface of HTNW, thereby led to the increase of the degradation rate of TC. Above process realized the electron reduction of Cr^{6+} on IM-CdS and hole oxidation of TC on HTNW, respectively, reducing the mutual interference between the two pollutants. Therefore, due to the occurrence of heterotopic reaction, IM-Cd/HT membrane exhibited a good balanced removal effect for TC and Cr^{6+}, more importantly, IM-Cd/HT membrane also realized the preferential reduction of Cr^{6+} under the interference of other ions.

3.8. Stability and self-cleaning

To reflect the photocatalytic stability of IM-Cd/HT membrane, five repeated Cr^{6+} removal experiments (Fig. 9) were done. After a routine photocatalytic experiment, IM-Cd/HT membrane was placed in room temperature air for 200 days, followed by five repeated experiments of Cr^{6+} removal. The repeated process was simple, just take out the membrane from the last reaction solution, rinsed it with DW for 3 times, and dried it for the next cycle. As shown in Fig. S10, compared with powder materials, it was obvious that membrane materials had faster and simpler recycling advantages. Moreover, the photocatalytic performance of the five cycles after 200 days of storage did not decrease significantly, and the mass before (0.4626 g) and after (0.4616 g) the reaction did not change much. The results of five cycles showed that the degradation rate was stable. This membrane material had convenient recycling and good photocatalytic stability. At the same time, the self-cleaning experiment using MB (Fig. S11) also showed that IM-Cd/HT membrane had good self-cleaning performance.

3.9. Flux and retention

Membrane flux and retention experiments were used to demonstrate the performance of membrane materials. In Fig. 10A, the four membranes had good water fluxes of 482.18 L $m^{-2}h^{-1}$, 382.42 L m^{-2} h^{-1}, 318.92 L m^{-2} h^{-1} and 295.25 L m^{-2} h^{-1}, which were related to the two-dimensional shape and good hydrophilicity of HTNW material. The water flux was basically consistent with the Cr^{6+} pollutant flux, and presented a downward trend. This may be due to the fact that CdS particles just filled the interlaced voids of 2D materials in HTNW membrane and increased the water flow path. At the same time, the presence of CdS surface polymer increased the specific surface area of NM-CdS and IM-CdS and increased the contact area of water flow. In addition, it can be seen from the Cr^{6+} rejection rate of the four materials that the Cr^{6+} rejection rate of HTNW membrane reached 42.26%, 50.28% (or 53.19%) after adding CdS (or NM-CdS), and 62.02% after adding IM-CdS. Among them, HTNW powder had more hydroxyl groups and higher specific surface area (33.00 m^2/g, Fig. S4), which was conducive to the retention of Cr^{6+} in a short time. A more intuitive retention effect of Cr^{6+} was shown in Fig. 10B. The color of the top of HTNW membrane changed from white to light yellow after Cr^{6+} retention experiment, which indicated that Cr^{6+} remained on the

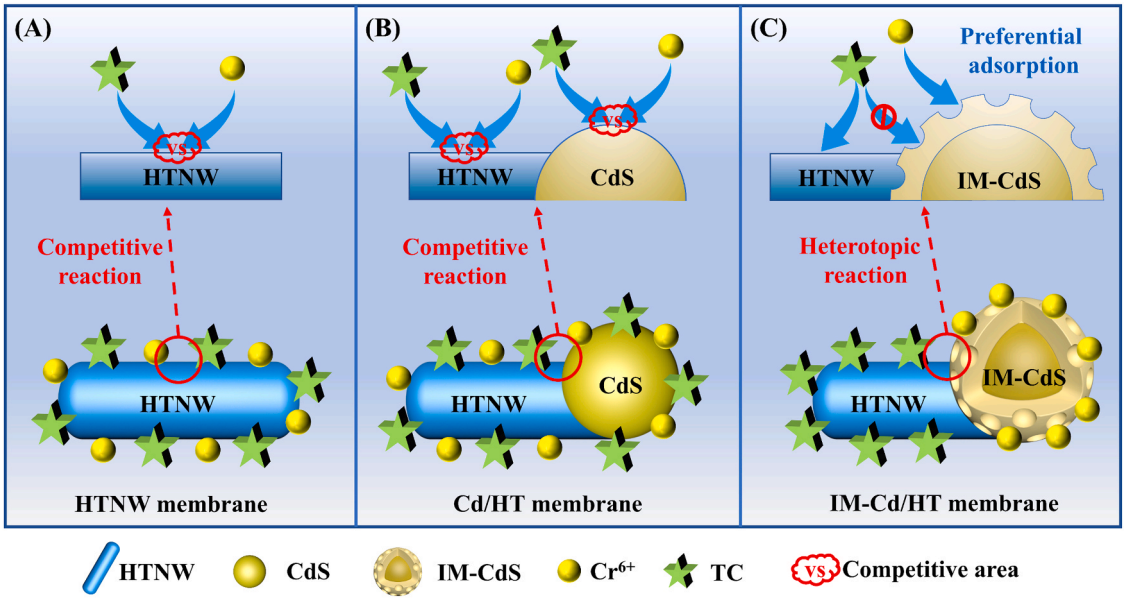

Fig. 8. Schematic diagram of possible adsorption competition of pollutants on different membranes in the binary TC and Cr^{6+}solution.

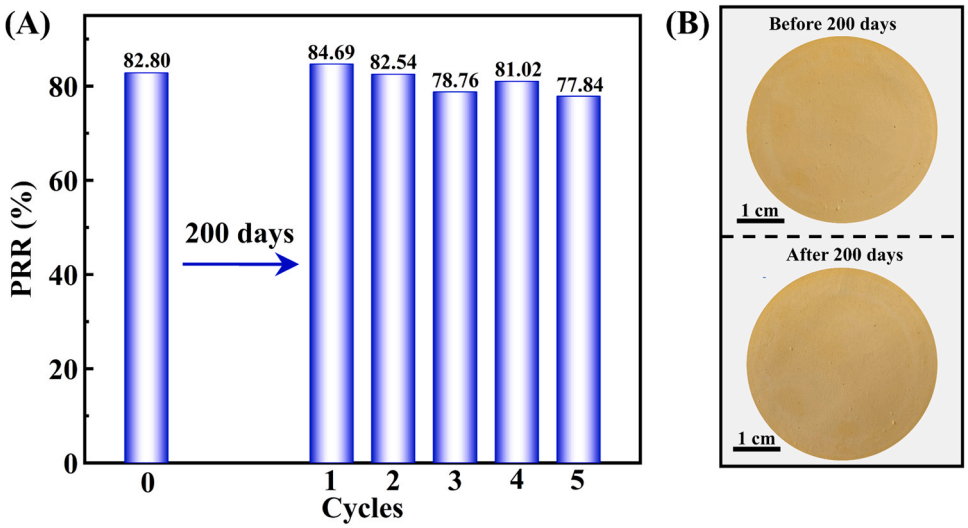

Fig. 9. Repeatability of Cr^{6+} removal by IM-Cd/HT membrane.

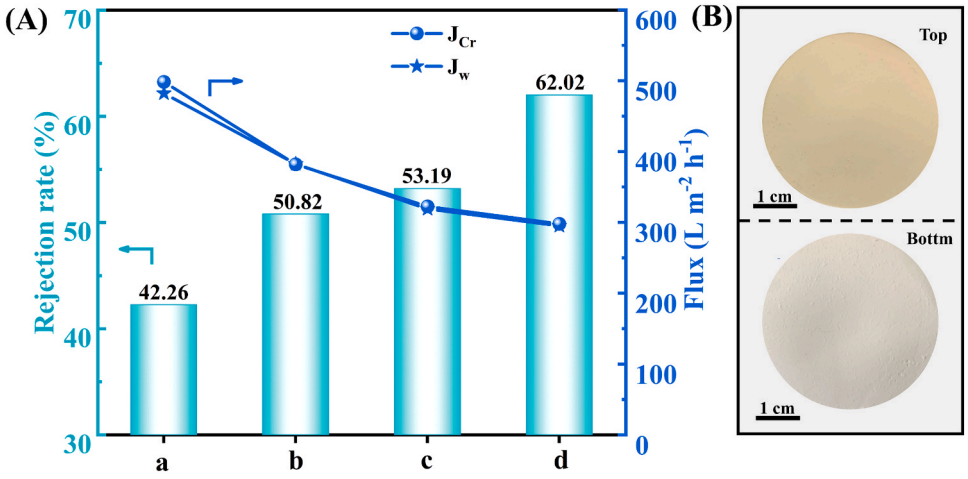

Fig. 10. (A) Flux and Cr^{6+} rejection rate of different membrane materials, pressure: 0.1 bar, (B) top and bottom of HTNW membrane after filtration of 50 mL Cr^{6+} single solution. (a. HTNW membrane, b. Cd/HT membrane, c. NM-Cd/HT membrane and d. IM-Cd/HT membrane).

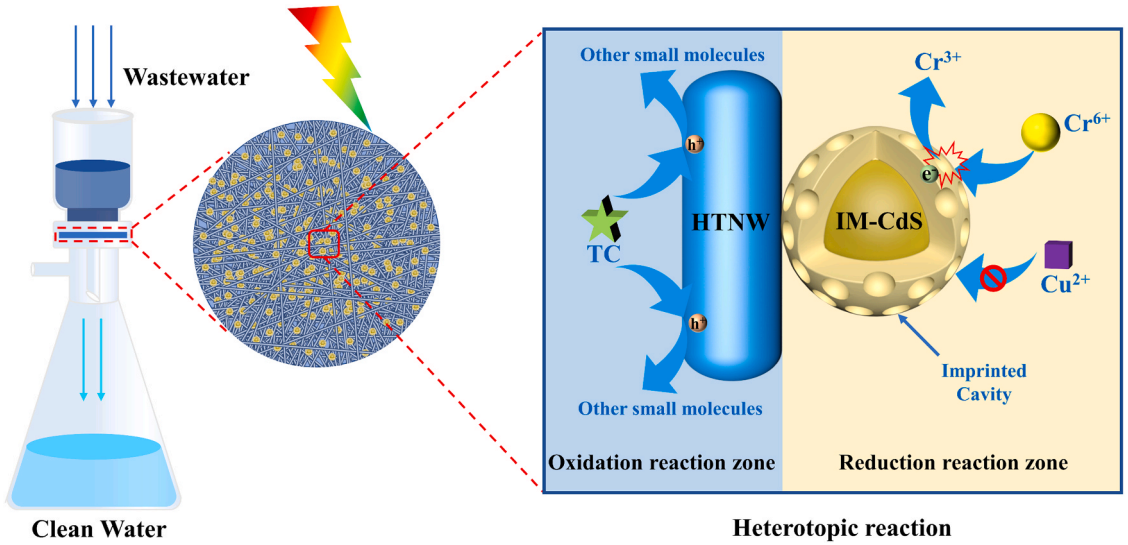

Fig. 11. Mechanism of membrane filtration and selective photocatalytic removal of pollutants.

membrane surface, while the color of the bottom remained white. In addition, IM-Cd/HT membrane had the best retention effect, which was due to the large S_{BET} of HTNW and IM-CdS on the one hand, and the existence of imprinted cavities on the other hand, both of them could achieve Cr^{6+} retention at the same time.

3.10. Mechanism

The possible mechanisms of membrane filtration process and synergistic selective photocatalytic removal of pollutants were shown in Fig. 11. In the process of pollutant filtration, Cr^{6+} would be trapped on the surface of IM-Cd/HT membrane to obtain clean filtrate. And the mechanism of synergistic selective photocatalytic removal was explored. In Fig. S12, the flat band potentials of HTNW and CdS were − 0.27 vs. SCE and − 1.18 vs. SCE, respectively. According to the Nernst equation [70], their flat band potentials were 0.39 eV and − 0.52 eV respectively. The slope of the model Schottky curve of the two materials was positive, both materials were n-type semiconductors, and their flat band potential was near the bottom of the conduction band, so the flat band potentials was approximately equal to the conduction band value [71,72]. Combined with the calculated band gap values, it can be calculated that the valence band values of HTNW and CdS were 4.03 eV and 1.82 eV, respectively. The detailed energy level positions were shown in Fig. S13. According to the reduction potentials of Cu^{2+}/Cu and Cr^{6+}/Cr^{3+}, CdS could reduce both Cu^{2+} and Cr^{6+}, while HTNW could only reduce Cr^{6+}, which was the same as the above experimental results.

In the process of synergistic selective photocatalytic removal of pollutants, Cr^{6+} and TC were enriched in the imprinted cavities of IM-CdS and HTNW, respectively, resulting in heterotopic reaction. TC could be degraded into some small molecules by using the holes generated by HTNW in oxidation reaction zone. And because of the existence of imprinted cavities, the electrons generated by CdS could preferentially reduce the heavy metal Cr^{6+} in reduction reaction zone. Therefore, IM-Cd/HT membrane could achieve efficient synergistic utilization of electrons and holes. Cr^{6+} could be selectively adsorbed by imprinted cavities on the surface of IM-CdS and then reduced by conduction band electrons, while Cu^{2+} could not be adsorbed by imprinted cavities. Meanwhile, the reduction potential of Cu^{2+} was higher, which led to the inability of the electrons in the HTNW conduction band to reduce Cu^{2+}, and further improved the selectivity of Cr^{6+}. Due to the occurrence of heterotopic reaction, IM-Cd/HT membrane exhibited a good balanced removal effect for TC and Cr^{6+}, more importantly, IM-Cd/HT membrane also realized the preferential reduction of Cr^{6+} under the interference of Cu^{2+}.

4. Conclusions

In conclusion, the IM-Cd/HT membrane was synthesized by using the stable inorganic oxidation type HTNW photocatalyst and the reduction type ion imprinted CdS photocatalyst. The results of XRD, FT-IR, SEM, TEM, EDS, XPS and nitrogen adsorption-desorption experiment indicated that the materials were successfully prepared. The photocatalysis experimental results showed that Cr^{6+} and TC reacted on the membrane in a heterotopic manner, Cr^{6+} was trapped into specific reaction site of IM-CdS for selective reduction, while TC migrated to HTNW for synergistic oxidation, and there was no interference between the two reactions. And the selectivity experiment showed that Cr^{6+} could be reduced preferentially by the membrane compared with other non-imprinted materials. Next, the stability and self-cleaning experiments showed that the membrane had good stability and self-cleaning performance. In addition, the membrane related experiments showed that the pure water flux and Cr^{6+} pollutant flux of the membrane reached about 2952 L m^{-2} h^{-1} bar^{-1}, and the effective retention of Cr^{6+} was increased by 1.47 times compared with the pure HTNW membrane. Therefore, the IM-Cd/HT membrane showed good heterotopic reaction effect, selectivity, stability, self-cleaning and retention effect. The design of imprinted photocatalytic membrane provides an effective strategy for the removal of coexisting heavy metal ions and antibiotic residues in water, and a new idea for the design of functional self-cleaning membrane.

CRediT authorship contribution statement

Ziyang Lu: Conceptualization, Resources, Writing – review & editing, Supervision. **Guosheng Zhou:** Methodology, Validation, Data curation, Writing – original draft. **Bing Li:** Writing – original draft. **Yangrui Xu:** Data curation. **Panpan Wang:** Validation. **Huan Yan:** Writing – review & editing. **Minshan Song:** Formal analysis. **Changchang Ma:** Investigation, Resources. **Song Han:** Validation. **Xinlin Liu:** Methodology, Resources, Project administration.

Declaration of Competing Interest

The authors declare that they have no known competing financial interests or personal relationships that could have appeared to influence the work reported in this paper.

Acknowledgements

This work was supported by National Natural Science Foundation of China (21908080), Natural Science Foundation of Jiangsu Province (BK20180884), Zhenjiang Key Research & Development Project (SH2018021), Jiangsu Government Scholarship for Overseas Studies (JS-2018-243 and JS-2018-241), Young Scientific and Technological Talents Support Project of Jiangsu Association for Science and Technology, and Jiangsu Collaborative Innovation Center of Technology and Material of Water Treatment.

Appendix A. Supporting information

Supplementary data associated with this article can be found in the online version at doi:10.1016/j.apcatb.2021.120787.

References

[1] M. Wu, X.C. Qiu, C. Chen, K. Chen, M. Li, H. Xu, X.Y. Wu, Y. Shimasaki, Y. Oshima, Short-term and persistent impacts of sublethal exposure to diazepam on behavioral traits and brain GABA levels in juvenile zebrafish (Danio rerio), Sci. Total. Environ. 740 (2020), 140392.

[2] L.S. Zhang, X.H. Jiang, Z.A. Zhong, L. Tian, Q. Sun, Y.T. Cui, X. Lu, J.P. Zou, S. L. Luo, Carbon nitride supported high-loading Fe single-atom catalyst for activating of peroxymonosulfate to generate $^1O_2$ with 100% selectivity, Angew. Chem. Int. Ed. 60 (2021) 1–6.

[3] M.L. Tang, Y.H. Ao, C. Wang, P.F. Wang, Rationally constructing of a novel dual Z-scheme composite photocatalyst with significantly enhanced performance for neonicotinoid degradation under visible light irradiation, Appl. Catal. B 270 (2020), 118918.

[4] D.M. Hausladen, A. Alexander-Ozinskas, C. McClain, S. Fendorf, Hexavalent chromium sources and distribution in California groundwater, Environ. Sci. Technol. 52 (2018) 8242–8251.

[5] X.H. Jiang, F. Yu, D.S. Wu, L. Tian, L.L. Zheng, L.S. Chen, P. Chen, L.S. Zhang, H. Zeng, Y. Chen, J.P. Zou, Isotypic heterojunction based on Fe-doped and terephthalaldehyde-modified carbon nitride for improving photocatalytic degradation with simultaneous hydrogen production, Chin. Chem. Lett. (2021), https://doi.org/10.1016/j.cclet.2021.01.1011.

[6] J. Yang, J.F. Jing, Y.F. Zhu, A full-spectrum porphyrin-fullerene D-A supramolecular photocatalyst with giant built-in electric field for efficient hydrogen production, Adv. Mater. 33 (2021), 2101026..

[7] Q. Zhang, G. Ying, C. Pan, Y. Liu, J. Zhao, Comprehensive evaluation of antibiotics emission and fate in the river basins of China: source analysis, multimedia modeling, and linkage to bacterial resistance, Environ. Sci. Technol. 49 (2015) 6772–6782.

[8] T.Y. Wang, S.X. Liu, W. Mao, Y.C. Bai, K. Chiang, K. Shah, J. Paz-Ferreiro, Novel Bi_2WO_6 loaded N-biochar composites with enhanced photocatalytic degradation of rhodamine B and Cr(VI), J. Hazard. Mater. 389 (2020), 121827.

[9] D. Blowes, Tracking hexavalent Cr in groundwater, Science 295 (2002) 2024–2025.

[10] G.P. Zhang, D.Y. Chen, N.J. Li, Q.F. Xu, H. Li, J.H. He, J.M. Lu, Preparation of $ZnIn_2S_4$ nanosheet-coated CdS nanorod heterostructures for efficient photocatalytic reduction of Cr(VI), Appl. Catal. B 232 (2018) 164–174.

[11] X. Lian, J. Zhang, Y. Zhan, Y. Zhang, S. Yang, Z. Chen, Y. Dong, W. Fang, X. Yi, Engineering $BiVO_4$@Bi_2S_3 heterojunction by cosharing bismuth atoms toward boosted photocatalytic Cr(VI) reduction, J. Hazard. Mater. 406 (2021), 124705.

[12] X.Q. He, G.J. Chen, Z.Y. Fang, W.J. Liang, B.D. Li, J.H. Tang, Y.G. Sun, L.P. Qin, Source identification of chromium in the sediments of the Xiaoqing River and Laizhou Bay: a chromium stable isotope perspective, Environ. Pollut. 264 (2020), 114686.

[13] M. Yoshinaga, H. Ninomiya, M.M.A. Al Hossain, M. Sudo, A.A. Akhand, N. Ahsan, M.A. Alim, M. Khalequzzaman, M. Iida, I. Yajima, N. Ohgami, M. Kato, A comprehensive study including monitoring, assessment of health effects and development of a remediation method for chromium pollution, Chemosphere 201 (2018) 667–675.

[14] B.W. Chen, L. Lin, L. Fang, Y. Yang, E.Z. Chen, K. Yuan, S.C. Zou, X.W. Wang, T. G. Luan, Complex pollution of antibiotic resistance genes due to beta-lactam and aminoglycoside use in aquaculture farming, Water Res. 134 (2018) 200–208.

[15] D. Li, S.Y. Zeng, M. He, A.Z. Gu, Water disinfection byproducts induce antibiotic resistance-role of environmental pollutants in resistance phenomena, Environ. Sci. Technol. 50 (2016) 3193–3201.

[16] T.P. Van Boeckel, J. Pires, R. Silvester, C. Zhao, J. Song, N.G. Criscuolo, M. Gilbert, S. Bonhoeffer, R. Laxminarayan, Global trends in antimicrobial resistance in animals in low- and middle-income countries, Science 365 (2019) 1266.

[17] Q. Yuan, L. Chen, M. Xiong, J. He, S.L. Luo, C.T. Au, S.F. Yin, Cu_2O/$BiVO_4$ heterostructures: synthesis and application in simultaneous photocatalytic oxidation of organic dyes and reduction of Cr(VI) under visible light, Chem. Eng. J. 255 (2014) 394–402.

[18] F. Chen, Q. Yang, Y.L. Wang, F.B. Yao, Y.H. Ma, X.D. Huang, X.M. Li, D.B. Wang, G. M. Zeng, H.Q. Yu, Efficient construction of bismuth vanadate-based Z-scheme photocatalyst for simultaneous Cr(VI) reduction and ciprofloxacin oxidation under visible light: Kinetics, degradation pathways and mechanism, Chem. Eng. J. 348 (2018) 157–170.

[19] F. He, Z.Y. Lu, M.S. Song, X.L. Liu, H. Tang, P.W. Huo, W.Q. Fan, H.J. Dong, X. Y. Wu, G.L. Xing, Construction of ion imprinted layer modified $ZnFe_2O_4$ for selective Cr (VI) reduction with simultaneous organic pollutants degradation based on different reaction channels, Appl. Surf. Sci. 483 (2019) 453–462.

[20] W. Zhao, J. Li, B.L. Dai, Z.P. Cheng, J.M. Xu, K.R. Ma, L.L. Zhang, N. Sheng, G. X. Mao, H.W. Wu, K.X. Wei, D.Y.C. Leung, Simultaneous removal of tetracycline and Cr(VI) by a novel three-dimensional AgI/$BiVO_4$ p-n junction photocatalyst and insight into the photocatalytic mechanism, Chem. Eng. J. 369 (2019) 716–725.

[21] J.P. Zou, Y. Chen, S.S. Liu, Q.J. Xing, W.H. Dong, X.B. Luo, W.L. Dai, X. Xiao, J. M. Luo, J. Crittenden, Electrochemical oxidation and advanced oxidation processes using a 3D hexagonal Co_3O_4 array anode for 4-nitrophenol decomposition coupled with simultaneous CO_2 conversion to liquid fuels via a flower-like CuO cathode, Water Res. 150 (2019) 330–339.

[22] W. Li, G. Zhou, X. Zhu, M. Song, Z. Lu, Magnetic assembly synthesis of high-efficiency recyclable flower-like MoS_2@Fe_3O_4@Cu_2O like-Z-scheme heterojunction towards efficient photodegradation of tetracycline, Appl. Surf. Sci. 555 (2021), 149730.

[23] Z.Y. Lu, J.Y. Peng, M.S. Song, Y. Liu, X.L. Liu, P.W. Huo, H.J. Dong, S.Q. Yuan, Z. F. Ma, S. Han, Improved recyclability and selectivity of environment-friendly MFA-based heterojunction imprinted photocatalyst for secondary pollution free tetracycline orientation degradation, Chem. Eng. J. 360 (2019) 1262–1276.

[24] M. Zhu, L.S. Zhang, S.S. Liu, D.K. Wang, Y.C. Qin, Y. Chen, W.L. Dai, Y.H. Wang, Q. J. Xing, J.P. Zou, Degradation of 4-nitrophenol by electrocatalysis and advanced oxidation processes using Co_3O_4@C anode coupled with simultaneous CO_2 reduction via SnO_2/CC cathode, Chin. Chem. Lett. 31 (2020) 1961–1965.

[25] Y.R. Xu, X.D. Zhu, H. Yan, P.P. Wang, M.S. Song, C.C. Ma, Z.R. Chen, J.Y. Chu, X. L. Liu, Z.Y. Lu, Hydrochloric acid-mediated synthesis of $ZnFe_2O_4$ small particle decorated one-dimensional PDI S-scheme heterojunction with excellent photocatalytic ability, Chin. J. Catal. (2021), https://doi.org/10.1016/S1872-2067(1021)63930-X.

[26] B. Gao, J.J. An, Y.P. Wang, J.D. Liu, L. Wang, M. Sillanpaa, Functional photoelectrocatalytic membrane fabricated from $ZnIn_2S_4$, PVDF and carbon fibre for continuous removal of tetracycline, J. Solid State Chem. 290 (2020), 121525.

[27] M. Owlad, M.K. Aroua, W.A.W. Daud, S. Baroutian, Removal of hexavalent chromium-contaminated water and wastewater: a review, Water Air Soil Pollut. 200 (2009) 59–77.

[28] A.O. Saf, S. Alpaydin, A. Coskun, M. Ersoz, Selective transport and removal of Cr (VI) through polymer inclusion membrane containing 5-(4-phenoxyphenyl)-6H-1,3,4-thiadiazin-2-amine as a carrier, J. Membr. Sci. 377 (2011) 241–248.

[29] Y.H. Shi, D.J. Wan, J.H. Huang, Y.D. Liu, J.S. Li, Stable LBL self-assembly coating porous membrane with 3D heterostructure for enhanced water treatment under visible light irradiation, Chemosphere 252 (2020), 126581.

[30] M. Yan, Y.L. Wu, X.L. Liu, Photocatalytic nanocomposite membranes for high-efficiency degradation of tetracycline under visible light: an imitated core-shell Au-TiO_2-based design, J. Alloy. Compd. 855 (2021), 157548.

[31] H.J. Zeng, Z.X. Yu, L.Y. Shao, X.H. Li, M. Zhu, Y.C. Liu, X.F. Feng, X.M. Zhu, Ag_2CO_3@UiO-66-NH_2 embedding graphene oxide sheets photocatalytic membrane for enhancing the removal performance of Cr(VI) and dyes based on filtration, Desalination 491 (2020), 114558.

[32] C. Yu, J. Lu, Z.Q. Hou, Z.F. Ma, X.Y. Lin, Z.Q. Dong, W.D. Xing, Y.S. Yan, Y.L. Wu, Mixed matrix membranes for rubidium-dependent recognition and separation: a synergistic recombination design based on electrostatic interactions, Sep. Purif. Technol. 255 (2021), 117727.

[33] H.R. Zhang, A.U. Mane, X.B. Yang, Z.J. Xia, E.F. Barry, J.Q. Luo, Y.H. Wan, J. W. Elam, S.B. Darling, Visible-light-activated photocatalytic films toward self-cleaning membranes, Adv. Funct. Mater. 30 (2020), 2002847.

[34] J.H. Huang, J.L. Hu, Y.H. Shi, G.M. Zeng, W.J. Cheng, H.B. Yu, Y.L. Gu, L.X. Shi, K. X. Yi, Evaluation of self-cleaning and photocatalytic properties of modified g-C_3N_4 based PVDF membranes driven by visible light, J. Colloid Interface Sci. 541 (2019) 356–366.

[35] E. Jeong, J. Byun, B. Bayarkhuu, S.W. Hong, Hydrophilic photocatalytic membrane via grafting conjugated polyelectrolyte for visible-light-driven biofouling control, Appl. Catal. B 282 (2021), 119587.

[36] I. Kolesnyk, J. Kujawa, H. Bubela, V. Konovalova, A. Burban, A. Cyganiuk, W. Kujawski, Photocatalytic properties of PVDF membranes modified with g-C_3N_4 in the process of Rhodamines decomposition, Sep. Purif. Technol. 250 (2020), 117231.

[37] L. Zhang, T.C.A. Ng, X.M. Liu, Q.L. Gu, Y.J. Pang, Z.X. Zhang, Z.Y. Lyu, Z.M. He, H. Y. Ng, J. Wang, Hydrogenated TiO_2 membrane with photocatalytically enhanced anti-fouling for ultrafiltration of surface water, Appl. Catal. B 264 (2020), 118528.

[38] U. Shareef, M. Waqas, Bisphenol A removal through low-cost kaolin-based Ag@TiO_2 photocatalytic hollow fiber membrane from the liquid media under visible light lrradiation, J. Nanomater. 2020 (2020), 3541797.

[39] X.W. Zhang, T. Zhang, J.W. Ng, D.D. Sun, High-performance multifunctional TiO_2 nanowire ultrafiltration membrane with a hierarchical layer structure for water treatment, Adv. Funct. Mater. 19 (2009) 3731–3736.

[40] X.W. Zhang, A.J. Du, P. Lee, D.D. Sun, J.O. Leckie, TiO_2 nanowire membrane for concurrent filtration and photocatalytic oxidation of humic acid in water, J. Membr. Sci. 313 (2008) 44–51.

[41] Z. Zhao, J. Tian, Y. Sang, A. Cabot, H. Liu, Structure, synthesis, and applications of TiO_2 nanobelts, Adv. Mater. 27 (2015) 2557–2582.

[42] L.H. Lou, R.J. Kendall, S. Ramkumar, Comparison of hydrophilic PVA/TiO_2 and hydrophobic PVDF/TiO_2 microfiber webs on the dye pollutant photo-catalyzation, J. Environ. Chem. Eng. 8 (2020), 103914.

[43] X.P. Li, Y.B. Chen, X.Y. Hu, Y.F. Zhang, L.J. Hu, Desalination of dye solution utilizing PVA/PVDF hollow fiber composite membrane modified with TiO_2 nanoparticles, J. Membr. Sci. 471 (2014) 118–129.

[44] S. Sakarkar, S. Muthukumaran, V. Jegatheesan, Evaluation of polyvinyl alcohol (PVA) loading in the PVA/titanium dioxide (TiO_2) thin film coating on polyvinylidene fluoride (PVDF) membrane for the removal of textile dyes, Chemosphere 257 (2020), 127144.

[45] F. He, Z.Y. Lu, M.S. Song, X.L. Liu, H. Tang, P.W. Huo, W.Q. Fan, H.J. Dong, X. Y. Wu, S. Han, Selective reduction of Cu^{2+} with simultaneous degradation of tetracycline by the dual channels ion imprinted POPD-$CoFe_2O_4$ heterojunction photocatalyst, Chem. Eng. J. 360 (2019) 750–761.

[46] J.F. Jing, J. Yang, Z.J. Zhang, Y.F. Zhu, Supramolecular zinc porphyrin photocatalyst with strong reduction ability and robust built-in electric field for highly efficient hydrogen production, Adv. Energy Mater. 11 (2021), 2101392.

[47] Z.Y. Lu, C. Fei, H. Ming, M.S. Song, Z.F. Ma, W.D. Shi, Y.S. Yan, J.Z. Lan, L. Fang, X. Peng, Microwave synthesis of a novel magnetic imprinted TiO_2 photocatalyst with excellent transparency for selective photodegradation of enrofloxacin hydrochloride residues solution, Chem. Eng. J. 249 (2014) 15–26.

[48] Z.Q. Ren, D.L. Kong, K.Y. Wang, W.D. Zhang, Preparation and adsorption characteristics of an imprinted polymer for selective removal of Cr(VI) ions from aqueous solutions, J. Mater. Chem. A 2 (2014) 17952–17961.

[49] A. Kumar, A. Balouch, A.A. Pathan, Abdullah, M.S. Jagirani, A.M. Mahar, M.-U.-H. Rajput, Novel chromium imprinted polymer: synthesis, characterization and analytical applicability for the selective remediation of Cr(VI) from an aqueous system, Int. J. Environ. Anal. Chem. 99 (2019) 454–473.

[50] Z.W. Zhu, S.J. Zhang, G.L. Chen, S.G. Meng, X.Z. Zheng, S.F. Chen, F.X. Zhang, Minimized Pt deposition on CdS simultaneously maximizes the performance of hydrogen production and aromatic alcohols oxidation, Appl. Surf. Sci. 564 (2021), 150446.

[51] S.J. You, G.U. Semblante, S.C. Lu, R.A. Damodar, T.C. Wei, Evaluation of the antifouling and photocatalytic properties of poly(vinylidene fluoride) plasma-grafted poly(acrylic acid) membrane with self-assembled TiO_2, J. Hazard. Mater. 237–238 (2012) 10–19.

[52] T.Y. Zhou, Y.B. Wang, T.T. Li, H.J. Li, C.W. Yang, D.S. Sun, D.D. Wang, C.B. Liu, G. B. Che, Fabricating magnetic hydrophilic molecularly imprinted resin with enhanced adsorption and recognition performance for targeted detecting chlorophenols in environmental water, Chem. Eng. J. 420 (2021), 129904.

[53] S. Leong, A. Razmjou, K. Wang, K. Hapgood, X. Zhang, H. Wang, TiO_2 based photocatalytic membranes: a review, J. Membr. Sci. 472 (2014) 167–184.

[54] Y.A.B. Neolaka, G. Supriyanto, H.S. Kusuma, Adsorption performance of Cr(VI)-imprinted poly(4-VP-co-MMA) supported on activated Indonesia (Ende-Flores) natural zeolite structure for Cr(VI) removal from aqueous solution, J. Environ. Chem. Eng. 6 (2018) 3436–3443.

[55] Y.A.B. Neolaka, Y. Lawa, J.N. Naat, A.A. Pau Riwu, H. Darmokoesoemo, G. Supriyanto, C.I. Holdsworth, A.N. Amenaghawon, H.S. Kusuma, A Cr(VI)-imprinted-poly(4-VP-co-EGDMA) sorbent prepared using precipitation polymerization and its application for selective adsorptive removal and solid phase extraction of Cr(VI) ions from electroplating industrial wastewater, React. Funct. Polym. 147 (2020), 104451.

[56] P. Shanmugam, K. Rajakumar, R. Boddula, R.C. Ngullie, W. Wei, J. Xie, E. Murugan, Heterogeneous form of poly (4-vinyl pyridine) beads based dendrimer stabilized Ag, Au and PdNPs catalyst for reduction of trypan blue, Mater. Sci. Energy Technol. 2 (2019) 532–542.

[57] J. Bian, Z.Q. Zhang, J.N. Feng, M. Thangamuthu, F. Yang, L. Sun, Z.J. Li, Y. Qu, D. Y. Tang, Z.W. Lin, F.B. Bai, J.W. Tang, L.Q. Jing, Energy platform for directed charge transfer in the cascade Z-Scheme heterojunction: CO_2 photoreduction without a cocatalyst, Angew. Chem. Int. Ed. 60 (2021) 20906–20914.

[58] L. Shang, B. Li, W. Dong, B. Chen, C. Li, W. Tang, G. Wang, J. Wu, Y. Ying, Heteronanostructure of Ag particle on titanate nanowire membrane with enhanced photocatalytic properties and bactericidal activities, J. Hazard. Mater. 178 (2010) 1109–1114.
[59] L.N. Chi, Y.J. Qian, J.Q. Guo, X.Z. Wang, H. Arandiyan, Z. Jiang, Novel g-C_3N_4/TiO_2/PAA/PTFE ultrafiltration membrane enabling enhanced antifouling and exceptional visible-light photocatalytic self-cleaning, Catal. Today 335 (2019) 527–537.
[60] Z.Y. Mu, S.Y. Chen, Y. Wang, Z.Q. Zhang, Z.J. Li, B.F. Xin, L.Q. Jing, Controlled construction of copper phthalocyanine/α-Fe_2O_3 ultrathin S-Scheme heterojunctions for efficiently photocatalytic CO_2 reduction under wide visible-light irradiation, Small Sci. (2021), 2100050.
[61] C. Yu, J. Lu, J.W. Dai, Z.Q. Dong, X.Y. Lin, W.D. Xing, Y.L. Wu, Z.F. Ma, Bio-inspired fabrication of Ester-functionalized imprinted composite membrane for rapid and high-efficient recovery of lithium ion from seawater, J. Colloid Interface Sci. 572 (2020) 340–353.
[62] S. Huang, B.F. Zheng, Z.Y. Tang, X.Q. Mai, T. Ouyang, Z.Q. Liu, CH_3OH selective oxidation to HCHO on Z-scheme Fe_2O_3/g-C_3N_4 hybrid: the rate-determining step of C-H bond scission, Chem. Eng. J. 422 (2021), 130086.
[63] Z.Y. Lu, G.S. Zhou, M.S. Song, X.L. Liu, H. Tang, H.J. Dong, P.W. Huo, F. Yan, P. Du, G.Z. Xing, Development of magnetic imprinted PEDOT/CdS heterojunction photocatalytic nanoreactors: 3-dimensional specific recognition for selectively photocatalyzing danofloxacin mesylate, Appl. Catal. B 268 (2019), 118433.
[64] Z. Zhu, C.C. Ma, K.S. Yu, Z.Y. Lu, Z. Liu, P.W. Huo, X. Tang, Y.S. Yan, Synthesis Ce-doped biomass carbon-based g-C_3N_4 via plant growing guide and temperature-programmed technique for degrading 2-Mercaptobenzothiazole, Appl. Catal. B 268 (2020), 118432.
[65] S. Huang, T. Ouyang, B.F. Zheng, M. Dan, Z.Q. Liu, Enhanced photoelectrocatalytic activities for CH_3OH-to-HCHO conversion on Fe_2O_3/MoO_3: Fe-O-Mo covalency dominates the intrinsic activity, Angew. Chem. Int. Ed. 60 (2021) 9546–9552.
[66] Z.Y. Lu, G.S. Zhou, M.S. Song, D.D. Wang, P.W. Huo, W.Q. Fan, H.J. Dong, H. Tang, F. Yan, G.Z. Xing, Magnetic functional heterojunction reactors with 3D specific recognition for selective photocatalysis and synergistic photodegradation in binary antibiotic solutions, J. Mater. Chem. A 7 (2019) 13986–14000.
[67] S. He, C. Yan, X.Z. Chen, Z. Wang, T. Ouyang, M.L. Guo, Z.Q. Liu, Construction of core-shell heterojunction regulating α-Fe_2O_3 layer on CeO_2 nanotube arrays enables highly efficient Z-scheme photoelectrocatalysis, Appl. Catal. B 276 (2020), 119138.
[68] X.H. Jiang, L.S. Zhang, H.Y. Liu, D.S. Wu, F.Y. Wu, L. Tian, L.L. Liu, J.P. Zou, S. L. Luo, B.B. Chen, Silver single atom in carbon nitride catalyst for highly efficient photocatalytic hydrogen evolution, Angew. Chem. Int. Ed. 59 (2020) 23112–23116.
[69] X.Y. Chu, Y. Qu, A. Zada, L.L. Bai, Z.J. Li, F. Yang, L.N. Zhao, G.L. Zhang, X.J. Sun, Z.D. Yang, L.Q. Jing, Ultrathin phosphate-modulated Co phthalocyanine/g-C_3N_4 heterojunction photocatalysts with single Co-N_4 (II) sites for efficient O_2 activation, Adv. Sci. 7 (2020), 2001543.
[70] T. Wang, C.C. Chiang, Y.L. Wu, C. Lin, Y.J. Cheng, Y.K. Hsieh, C.F. Wang, C. Huang, Characteristics of elemental carbon overlayers over hematite electrodes prepared by electrodeposition with organic acid additives, Appl. Catal. B 207 (2017) 1–8.
[71] H.J. Dong, Y. Zuo, N. Song, S.H. Hong, M.Y. Xiao, D.Q. Zhu, J.X. Sun, G. Chen, C. M. Li, Bimetallic synergetic regulating effect on electronic structure in cobalt/vanadium co-doped carbon nitride for boosting photocatalytic performance, Appl. Catal. B 287 (2021), 119954.
[72] W.L. Shi, C. Liu, M.Y. Li, X. Lin, F. Guo, J.Y. Shi, Fabrication of ternary Ag_3PO_4/$Co_3(PO_4)_2$/g-C_3N_4 heterostructure with following Type II and Z-scheme dual pathways for enhanced visible-light photocatalytic activity, J. Hazard. Mater. 389 (2020), 121907.